Journal of ELECTRONIC MATERIALS, Vol. 38, No. 9, 2009
DOI: 10.1007/s11664-009-0835-y
© 2009 The Author(s). This article is published with open access at Springerlink.com
Regular Issue Paper

Characterization of $Zn_{1-x}Mg_xO$ Films Prepared by the Sol–Gel Process and Their Application for Thin-Film Transistors

CHIEN-YIE TSAY,[1,3] MIN-CHI WANG,[1] and SHIN-CHUAN CHIANG[2]

1.—Department of Materials Science and Engineering, Feng Chia University, Taichung, Taiwan 407, ROC. 2.—Research Alliance, Taiwan TFT LCD Association (TTLA), Hsinchu, Taiwan 310, ROC. 3.—e-mail: cytsay@fcu.edu.tw

Transparent semiconductor thin films of $Zn_{1-x}Mg_xO$ ($0 \le x \le 0.36$) were prepared using a sol–gel process; the crystallinity levels, microstructures, and optical properties affected by Mg content were studied. The experimental results showed that addition of Mg species in ZnO films markedly decreased the surface roughness and improved transparency in the visible range. A $Zn_{1-x}Mg_xO$ film with an x-value of 0.2 exhibited the best average transmittance, namely 93.7%, and a root-mean-square (RMS) roughness of 1.63 nm. Therefore, thin-film transistors (TFTs) with a $Zn_{0.8}Mg_{0.2}O$ active channel layer were fabricated and found to have n-type enhancement mode. The $Zn_{0.8}Mg_{0.2}O$ TFT had a field-effect mobility of 0.1 cm^2/V s, threshold voltage of 6.0 V, and drain current on/off ratio of more than 10^7.

Key words: Transparent oxide semiconductors, $Zn_{1-x}Mg_xO$, sol–gel process, thin-film transistors

INTRODUCTION

Wide-bandgap (>3 eV) metal oxides such as zinc oxide (ZnO), tin oxide (SnO_2) and indium tin oxide (ITO) have been extensively used for optoelectronic devices. Among these materials, ZnO is nontoxic and has high transparency and high crystallinity. When prepared in the low-temperature region, ZnO is a promising candidate for transparent field-effect transistors (TFETs) and transparent electronic circuit applications. Its unique electrical and optical properties have made it popular for use in varistors, chemical sensors, and piezoelectric devices. Recently, interest in ZnO thin films has focused on solar cell and flat-panel display applications, such as the window layer for thin-film solar cells, transparent conductive layer for touch panels, and active channel layer for thin-film transistors (TFTs). ZnO is an n-type oxide semiconductor material with a direct wide bandgap of 3.3 eV. Its electrical characteristics can be controlled by doping or incorporating ternary elements such as Al, Ga, and In.[1] The carrier mobility of pure ZnO exceeds the field-effect mobility of the hydrogenated amorphous silicon (a-Si:H) that serves as the active channel layer in typical TFT arrays. Additionally, transparent semiconductor ZnO thin films can be prepared in air under atmospheric pressure. Because ZnO may replace hydrogenated amorphous silicon as an active layer, it is presently attracting much attention.

The solution-based process offers a simple, low-cost, and large-area thin-film deposition method as an alternative to the vacuum deposition techniques of physical or chemical vapor deposition (PVD or CVD). Metal oxide semiconductors formed from the solution process might enable maskless processes, such as inkjet printing,[2] to improve the manufacturing throughput of microelectronic devices. The sol–gel process is a solution process that is commonly used for polycrystalline oxide thin-film deposition. ZnO-based semiconductor films have been used as the active channel layer in TFTs.[3–6] Kwon et al.[7] indicated that control of the carrier density of the active channel layer in ZnO-based TFTs is a challenge because the active channel layer supplies high carrier density that will conduct when an applied gate voltage is absent. The ionic radius of

(Received July 16, 2008; accepted April 25, 2009; published online May 22, 2009)

Mg^{2+} (0.65 Å) is smaller than that of Zn^{2+} (0.74 Å), and thus the limit of solid solubility of MgO in ZnO can approach 40 at.%.[8,9] The incorporation of Mg into ZnO films tends to decrease both the amount of interstitial oxygen vacancies[10] and the electron density.[11] Many reports have demonstrated that the solubility limit of Mg in $Zn_{1-x}Mg_xO$ films strongly depends on the deposition or growth technique, e.g., pulsed laser deposition (PLD),[9,12] sputtering,[13] metalorganic vapor-phase epitaxy (MOVPE)[8] or sol–gel process.[14,15] Recently, several reports have discussed the active channel layer of ZnO-based TFTs prepared by solution-based processes; for example, Norrs et al.[16] fabricated a ZnO transparent TFT in which the active channel layer was prepared by spin-coating. The TFT exhibited a mobility of 0.2 cm^2/V s. Cheng et al.[17] also fabricated a transparent ZnO TFT using a combination of sol–gel and chemical bath deposition methods. The optimum device had a mobility of 0.67 cm^2/V s. Lee et al.[18] used dip coating to deposit $Zn_{1-x}Mg_xO$ films. At $x = 0.2$, the active layer of that TFT showed an on/off current ratio of 10^6. Furthermore, Chang et al.[19] developed a high-performance zinc tin oxide (ZTO) TFT in which an amorphous semiconductor thin film was deposited by spin coating.

In the present study, transparent semiconductors of $Zn_{1-x}Mg_xO$ thin films were prepared using a sol–gel process, and the effects of Mg content on crystallinity, microstructure, and optical properties were investigated. Moreover, single-phase, defect-free $Zn_{1-x}Mg_xO$ films with good surface flatness were fabricated; further examination showed their electrical characteristics to be suitable for TFTs.

EXPERIMENTAL

For synthesis of $Zn_{1-x}Mg_xO$ sols, the x values of the Mg^{2+} molar fraction was varied from 0 to 0.36. A mixture of zinc acetate dehydrate $[Zn(CH_3COO)_2 \cdot 2H_2O]$ and magnesium acetate tetrahydrate $[Mg(CH_3COO)_2 \cdot 4H_2O]$ was dissolved in a solution of 2-methoxyethanol and monoethanolamine (MEA). The molar ratio of MEA to metal ions in the $Zn_{1-x}Mg_xO$ sols was maintained at 1.0, and the concentration of metal ions was controlled at 0.75 mol/L. The complex solution was stirred for 2 h at 60°C, after which a clear and homogenous sol was obtained. Each of the $Zn_{1-x}Mg_xO$ gel films was coated onto alkali-free glass (Corning 1737, 5 cm × 5 cm) using the spin-coating method at a speed of 3000 rpm for 30 s. The as-coated films were preheated at 300°C for 10 min immediately after coating. After repeating the coating procedure three times, the films were annealed in air in a tube furnace at 500°C for 1 h.

The crystallinity of pure ZnO and Mg incorporated ZnO thin films after annealing was determined by glancing-angle x-ray diffraction (GAXRD). These diffracted patterns were examined on a MAC Science MXP3 diffractometer with a glancing incident angle of 1°. The surface morphology and microstructure of the $Zn_{1-x}Mg_xO$ films were observed using scanning electron microscopy (SEM, HITACHI S-4800, Japan). Each film's surface roughness was analyzed using scanning probe microscopy (SPM, Digital Instrument NS4/D3100CL, Germany). Moreover, optical transmittance spectra of these films were examined by a ultraviolet (UV)-visible spectrophotometer (Mini-D2T, Ocean Optics Inc., USA).

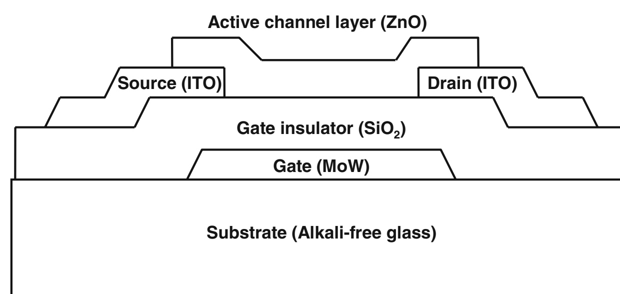

Fig. 1. Schematic cross-sectional structure of the TFT with ZnO:Mg thin film as active channel layer.

The ZnO:Mg film with the best performance in this study (a defect-free polycrystalline thin film with a single phase and uniform thickness) was evaluated for use as the active channel layer of a TFT application. A bottom-gate structure device (as shown in Fig. 1) was fabricated by a hybrid method that combined the standard microelectronic fabrication process with the sol–gel process. Figure 1 shows a schematic diagram of this device, which functions as a TFT and that used the ZnO:Mg thin film as its active channel layer. The fabrication procedure was as follows. A molybdenum-tungsten alloy (MoW) thin film with a thickness of 100 nm was deposited and patterned onto an alkali-free glass substrate. The thin film constituted the bottom gate electrode. A 300 nm thickness of silicon dioxide (SiO_2), prepared by plasma-enhanced chemical vapor deposition (PECVD), served as the gate insulator. A 100 nm thickness of indium tin oxide (ITO) thin film was sputtered onto the device and then patterned by a conventional photolithography process into a source and a drain. The channel length and width of the TFT device were offset at 500 μm and 60 μm, respectively. Finally, a ZnO-based semiconductor thin film was spin-coated onto the multilayer MoW/SiO_2/ITO structure; it was patterned by a photolithography and wet etching process to finish the ZnO:Mg TFT. An HP 4155B semiconductor parameter analyzer was used in a darkroom to examine the current–voltage (I–V) characteristics of the transistors.

RESULTS AND DISCUSSION

XRD patterns of pure ZnO and Mg-incorporated ZnO films are presented in Fig. 2. These patterns correspond to three main diffraction peaks of ZnO:

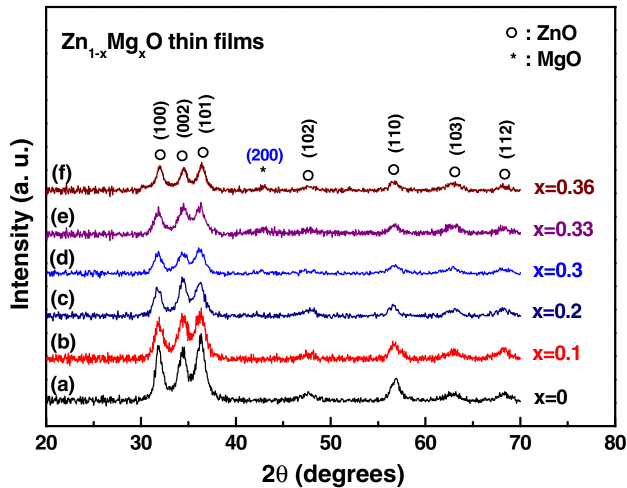

Fig. 2. XRD patterns of $Zn_{1-x}Mg_xO$ thin films ($0 \leq x \leq 0.36$) annealed in air at 500°C for 1 h.

Table I. Microstructure and Optical Properties of $Zn_{1-x}Mg_xO$ Thin Films

x in $Zn_{1-x}Mg_xO$	0	0.1	0.2	0.3	0.33	0.36
Average crystallite size (nm)	8.9	8.8	8.7	8.4	8.5	8.4
RMS roughness (nm)	16.24	7.81	1.63	1.97	2.79	3.82
Average transmittance (%)	86.4	90.8	93.7	92.7	92.5	88.3
Optical bandgap (eV)	3.24	3.36	3.51	3.52	3.47	3.47

the (100), (002), and (101) planes. All $Zn_{1-x}Mg_xO$ ($x \approx 0$ to 0.36) gel films were preheated at 300°C and then annealed at 500°C, which yielded polycrystalline films with a hexagonal wurzite structure (Zincite, JCPDS 36-1451). These x-ray diffractographs show that the intensity values of diffraction peaks decrease with increasing Mg content, i.e., Mg incorporated within the ZnO films degrades film crystallinity. The $Zn_{0.8}Mg_{0.2}O$ film shows a highly c-axis-oriented (002) peak (curve c in Fig. 2). To estimate the average crystallite size (d) of these samples, Scherrer's formula[20] is used:

$$d = \frac{0.9\lambda}{B\cos\theta_B}, \quad (1)$$

where λ is the x-ray wavelength (1.54 Å), θ_B is the Bragg diffraction angle, and B is the full-width at half-maximum (FWHM) of θ_B. The calculated average crystallite size of the $Zn_{1-x}Mg_xO$ films exhibited in Table I shows that Mg-incorporated ZnO thin films have a slightly reduced average grain size. In the XRD patterns of $Zn_{0.7}Mg_{0.3}O$, $Zn_{0.67}Mg_{0.33}O$ and $Zn_{0.64}Mg_{0.36}O$ films (curves d to f in Fig. 2) a weak diffraction signal at $2\theta = 42.9°$ corresponds to the (200) plane of the MgO cubic phase. The results show that, when the Mg content is more than 30 at.%, the MgO phase becomes segregated. Previous reports have demonstrated the high solubility of the Mg ion in ZnO films. For example, Ohtomo et al.[21] reported that the soluble range of the epitaxial $Zn_{1-x}Mg_xO$ films' growth by PLD was from 0.25 to 0.33. Also, Zhao et al.[14] demonstrated that, when the Mg content exceeded 0.36, MgO phase segregation would occur at 800°C. In their study, the $Zn_{1-x}Mg_xO$ films were fabricated by the sol–gel process.

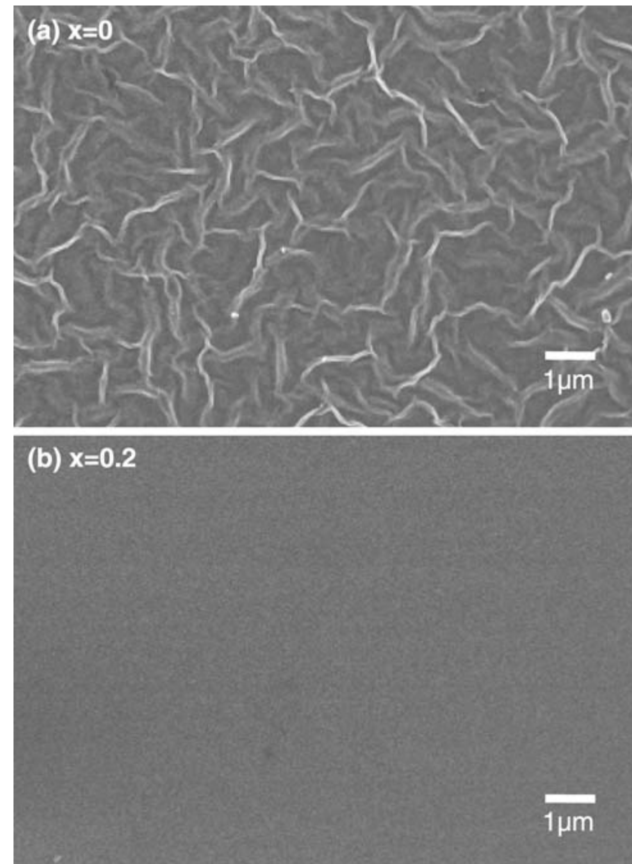

Fig. 3. SEM micrographs of surface morphology of (a) pure ZnO and (b) $Zn_{0.8}Mg_{0.2}O$ thin films.

On the vertical SEM micrograph of the annealed pure ZnO film one can observe fiber-like streaks or wrinkles (Fig. 3a). However, these features are absent from the samples that incorporate Mg, e.g., the image of the $Zn_{0.8}Mg_{0.2}O$ film shown in Fig. 3b. The fiber-like streaks or wrinkles are induced by short OH and/or OR groups, as a previous report has explained.[22] However, in the present study, magnesium acetate tetrahydrate is used as a source of Mg ions, and it can provide sufficient OH groups. Thus, $Zn_{1-x}Mg_xO$ thin films can be produced with relatively smooth surfaces.

SPM images of the $Zn_{1-x}Mg_xO$ thin films are shown in Fig. 4. The surface morphologies show the influence of the Mg incorporation into the ZnO thin films. It is apparent that a reduction of surface

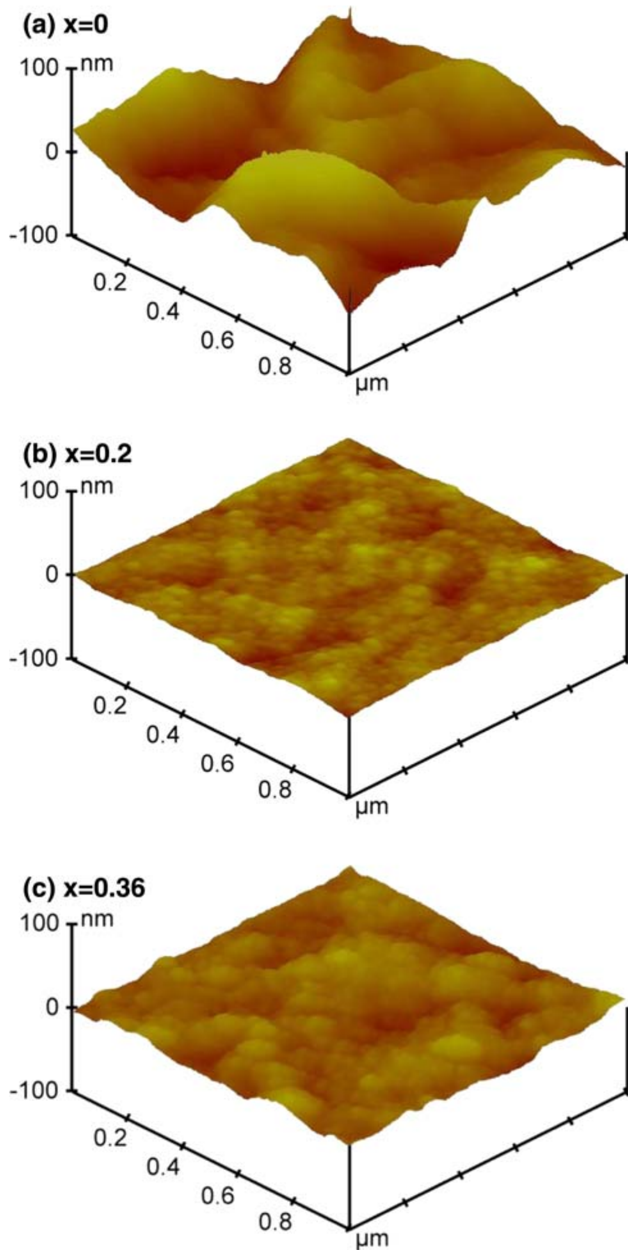

Fig. 4. SPM images of $Zn_{1-x}Mg_xO$ thin films: (a) $x = 0$, (b) $x = 0.2$, and (c) $x = 0.36$.

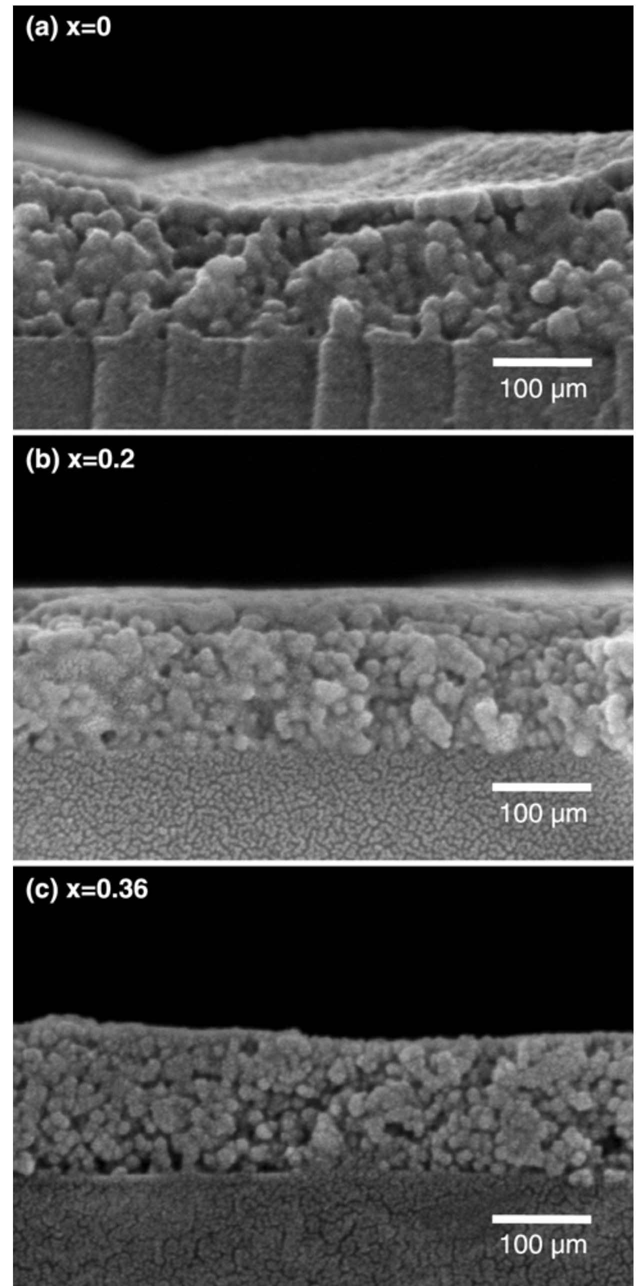

Fig. 5. SEM micrographs of cross-sections of $Zn_{1-x}Mg_xO$ thin films: (a) $x = 0$, (b) $x = 0.2$, and (c) $x = 0.36$.

roughness results from a decrease in the average crystallite size in the ZnO thin films after Mg substitution. Table I gives the values of RMS roughness of the $Zn_{1-x}Mg_xO$ thin films. A significant improvement of surface roughness with Mg incorporation can be observed. RMS roughness decreased as Mg concentration went up to $x = 0.2$ but increased with concentration greater than that. That is, the $Zn_{0.8}Mg_{0.2}O$ thin film exhibited the smallest RMS value (1.63 nm) of all the annealed $Zn_{1-x}Mg_xO$ thin films investigated in this study. However, the phase-segregated impurities of the $x = 0.3$ to 0.36 samples could possibly degrade the surface textures of those thin films.

Cross-sectional SEM micrographs of the $Zn_{1-x}Mg_xO$ thin films are shown in Fig. 5. Figure 5a shows an SEM micrograph of the ZnO film that shows its average thickness to be about 140 nm. Two SEM micrographs of the nanocrystalline $Zn_{1-x}Mg_xO$ films ($x = 0.2$ and 0.36) are shown in Fig. 5b and c, respectively. They show that the thickness of a typical incorporated film is about 150 nm, and that addition of Mg species to the ZnO films markedly improves the surface flatness and enhances the uniformity of the film thickness. These SEM images (Fig. 5) also reveal that Mg-incorporated ZnO films can reduce the average crystallite

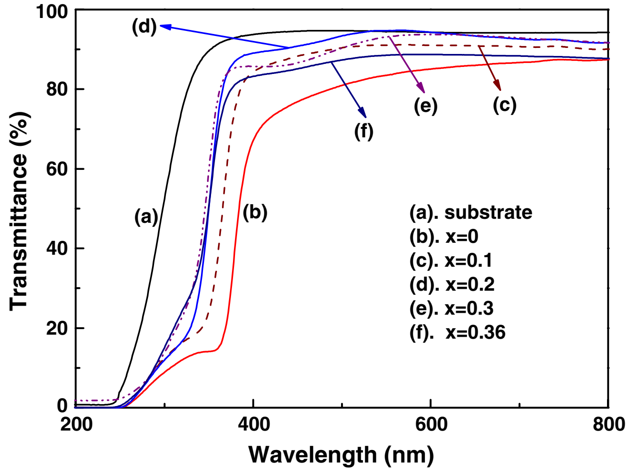

Fig. 6. Optical transmittance spectra of pure ZnO and Mg-incorporated ZnO thin films.

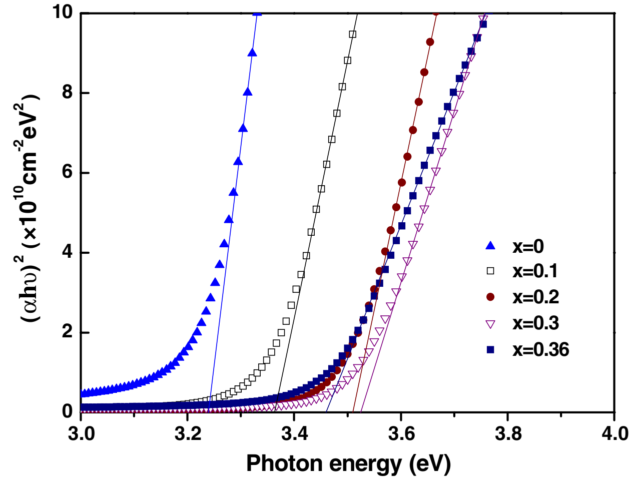

Fig. 7. Plot of $(\alpha h\nu)^2$ versus photon energy of pure ZnO and Mg-incorporated ZnO thin films.

size; this result agrees with XRD measurements. In addition, microscopy of the $Zn_{0.64}Mg_{0.36}O$ film, as shown in Fig. 5c, reveal a porous and noncompact microstructure. That film exhibited poor quality with an x-value over 0.3.

Figure 6 shows the optical properties of the $Zn_{1-x}Mg_xO$ thin films at room temperature. All samples show sharp absorption edges in the UV region; this absorption edge shifted to shorter wavelengths when Mg was incorporated in the ZnO thin film. A previous study reported that the absorption maxima of $Zn_{1-x}Mg_xO$ films blue-shifted as a function of Mg content.[15] The average transmittance in the visible range for the pure ZnO film is about 86.4%, and it exhibits an absorption edge approaching 362 nm (curve b in Fig. 6). Table I also presents average transmittance for wavelengths from 500 nm to 700 nm; this reveals that Mg-incorporated samples show higher transparency compared with the pure ZnO sample. However, the transmittance of higher Mg content samples, when $x \geq 0.3$, shows a slight decrease compared with the $x = 0.2$ sample. This result is in good agreement with the results of XRD, SEM, and SPM and relates to Mg phase segregation. In this study, the $Zn_{0.8}Mg_{0.2}O$ sample exhibits the best transparency (namely 93.7%) among the Mg-incorporated samples. This represents an increase of about 8.5% over the pure ZnO sample.

In a direct-bandgap semiconductor, the absorption edge can be analyzed by the relation[23]:

$$(\alpha h\nu) = A(h\nu - E_g)^{1/2}, \qquad (2)$$

where α is the absorption coefficient, $h\nu$ is the photon energy, A is a constant, and E_g is the optical bandgap. The absorption coefficient (α) in the UV region of these $Zn_{1-x}Mg_xO$ thin films can be calculated from $I = I_0e^{-\alpha t}$,[24] where I is the intensity of the transmitted light, I_0 is the intensity of incident light, and t is the thickness of the $Zn_{1-x}Mg_xO$ film.

Figure 7 shows a plot of $(\alpha h\nu)^2$ versus photon energy. These curves were evaluated from the transmittance spectra in Fig. 6. Thus, it is possible to extrapolate the optical bandgap of $Zn_{1-x}Mg_xO$ thin films. The optical bandgap (E_g) values listed in Table I show that the bandgap increased with Mg content, from 3.24 eV to 3.51 eV, for $0 \leq x \leq 0.2$. Tan et al. have indicated that the optical bandgap blueshift is caused by the poor crystallinity of ZnO films.[25] Moreover, at x values exceeding 0.3, E_g approaches 3.47 eV. It is possible that film defects and phase separation cause this effect.

An MgO phase separated from the $Zn_{1-x}Mg_xO$ film can degrade its crystallinity, electrical characteristics, and optical properties. Thus, according to this research, in order to make sure the $Zn_{1-x}Mg_xO$ film possesses a pure hexagonal crystal structure, the content of Mg^{2+} should not be greater than $x = 0.3$. A defect-free, single-phase polycrystalline semiconductor thin film with uniform thickness and a flat surface can serve as the active channel layer for carrier propagation from source to drain. As previously discussed, the $Zn_{0.8}Mg_{0.2}O$ thin film produced in this study possessed such good characteristics. Therefore, TFTs with a $Zn_{0.8}Mg_{x0.2}O$ active channel layer were fabricated and their current–voltage (I–V) characteristics were evaluated. Two cross-sectional views of a $Zn_{0.8}Mg_{0.2}O$ TFT are shown in Fig. 8. The images illustrate that a polycrystalline semiconductor $Zn_{0.8}Mg_{0.2}O$ film was successfully deposited on the multilayer structure. There were no voids or pores in or between the ITO/$Zn_{0.8}Mg_{0.2}O$ and SiO_2/$Zn_{0.8}Mg_{0.2}O$ interfaces.

Figure 9a shows the drain current-drain voltage (I_D–V_D) characteristics for a $Zn_{0.8}Mg_{0.2}O$ TFT. V_G was increased from 0 V to 100 V in 20 V steps. The plot shows that the field-effect transistor operates in n-type enhancement mode, and the drain current increases with positive gate bias. Furthermore, the slope of each I_D curve is flat and exhibits hard

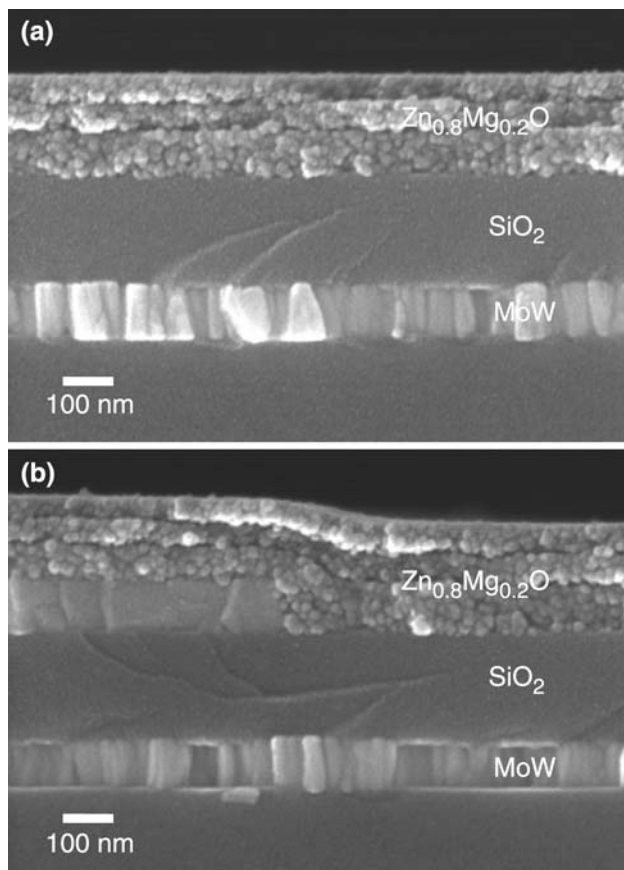

Fig. 8. Local cross-section view of $Zn_{0.8}Mg_{0.2}O$ TFT: (a) the active channel region and (b) the source electrode region.

saturation for the large-V_D region. Hoffman et al.[26] indicated that hard saturation for the entire layer of the ZnO-based active channel layer could deplete free electrons, and that a device that possesses large drain current is desirable for most circuit applications. Indeed, multiple interfaces are observed within the polycrystalline semiconductor layer of the $Zn_{0.8}Mg_{0.2}O$ TFT (Fig. 8a and b). Any macrodefects on the transferring path of the carrier would cause the TFT to exhibit low on-currents and large gate bias relative to the active channel of the ZnO-based TFT deposited by PVD[27,28] or CVD.[29,30]

Typical transfer characteristics [log(I_D)–V_G] and gate leakage current [log(I_G)–V_G] of the same device are shown in Fig. 9b. These numbers were measured at fixed V_D of 30 V. This log(I_D)–V_G curve reveals a maximum drain current on/off ratio of more than 10^7. From this figure one can observe that the gate leakage current (I_G) slightly increased with increasing gate voltage. The magnitude of I_G was below 10^{-10} A; therefore, the SiO_2 gate insulator was usefully utilized in this device. The inset of Fig. 9b shows an extrapolation of the linear portion of an $(I_D)^{1/2}$–V_G curve that estimates a threshold voltage (V_{th}) of 6.0 V. Moreover, the field-effect mobility (μ_{FEsat}) of the drain current in the

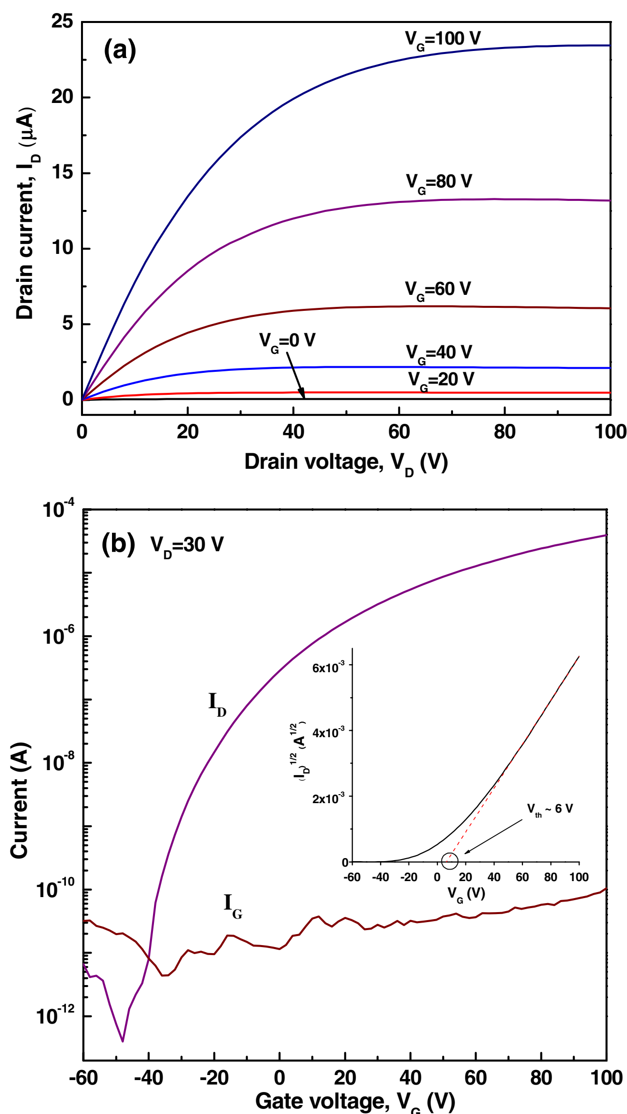

Fig. 9. (a) I_D–V_D curve (output characteristics); (b) log(I_D)–V_G (transfer characteristics) and log(I_G)–V_G curves of $Zn_{0.8}Mg_{0.2}O$ TFT. The inset shows how the threshold voltage (V_{th}) was defined by fitting a straight line, and then intercepting the x-axis of the $(I_D)^{1/2}$–V_G curve.

saturated region was determined from the following equation[31]:

$$I_{D(sat)} = \mu_{FEsat} C_I \left(\frac{W}{2L}\right)(V_G - V_{th})^2, \quad (3)$$

where C_I is the unit capacitance of the gate insulator, and W and L are the channel width and length, respectively. The μ_{FEsat} of the $Zn_{0.8}Mg_{0.2}O$ TFT was calculated to be 0.1 cm^2/V s.

CONCLUSIONS

$Zn_{1-x}Mg_xO$ (x = 0 to 0.36) thin films have been successfully deposited on alkali-free glass by the sol–gel process. The results show that Mg^{2+} incorporation within ZnO thin films markedly decreased

surface roughness, improved transparency in the visible range, and gave a finer microstructure than that of a pure ZnO film. The optical bandgap of $Zn_{1-x}Mg_xO$ thin films can be tuned from 3.24 eV (x = 0) to 3.51 eV (x = 0.2) by varying the Mg content. The $Zn_{0.8}Mg_{0.2}O$ film exhibited the best transparency, 93.7%, and its RMS roughness value was 1.63 nm. When the Mg content exceeded 0.3 (x value), MgO phase segregation occurred. This impurity phase caused the film quality to degrade. In this study, a TFT with a $Zn_{0.8}Mg_{0.2}O$ active channel layer was fabricated using the sol–gel process. The resulting field-effect device exhibited n-type enhancement mode behavior and had a field-effect mobility of 0.1 $cm^2 V^{-1} s^{-1}$, threshold voltage of 6.0 V, and drain current on/off ratio of more than 10^7.

ACKNOWLEDGEMENTS

The authors gratefully acknowledge the financial support of the Taiwan TFT-LCD Association (TTLA) under Contract No. A643TT1000-S11.

OPEN ACCESS

This article is distributed under the terms of the Creative Commons Attribution Noncommercial License which permits any noncommercial use, distribution, and reproduction in any medium, provided the original author(s) and source are credited.

REFERENCES

1. D.P. Norton, Y.W. Heo, M.P. Ivill, K. Ip, S.J. Pearton, M.F. Chisholm, and T. Steiner, *Mater. Today* 6, 34 (2004). doi:10.1016/S1369-7021(04)00287-1.
2. D.H. Lee, Y.J. Chang, W. Stickle, and C.H. Chang, *Electrochem. Solid-State Lett.* 10, K51 (2007). doi:10.1149/1.2773531.
3. P.F. Carcia, R.S. McLean, M.H. Reilly, and G. Nunes Jr., *Appl. Phys. Lett.* 82, 1117 (2003). doi:10.1063/1.1553997.
4. R.L. Hoffman, *J. Appl. Phys.* 95, 5813 (2004). doi:10.1063/1.1712015.
5. E. Fortunato, P. Barquinha, A. Pimentel, A. Goncalves, A. Marques, L. Pereira, and R. Martins, *Thin Solid Films* 487, 205 (2005). doi:10.1016/j.tsf.2005.01.066.
6. P.K. Shin, Y. Aya, T. Ikegami, and K. Ebihara, *Thin Solid Films* 516, 3767 (2008). doi:10.1016/j.tsf.2007.06.068.
7. Y. Kwon, Y. Li, Y.W. Heo, M. Jones, P.H. Hollyway, D.P. Norton, Z.V. Park, and S. Li, *Appl. Phys. Lett.* 84, 2685 (2004). doi:10.1063/1.1695437.
8. W.I. Park, G.C. Yi, and H.M. Jang, *Appl. Phys. Lett.* 79, 2022 (2001). doi:10.1063/1.1405811.
9. J.W. Kim, H.S. Kang, J.H. Kim, S.Y. Lee, J.K. Lee, and M. Nastasi, *J. Appl. Phys.* 100, 033701 (2006). doi:10.1063/1.2219153.
10. Y. Ogawa and S. Fujihara, *Phys. Status Solidi* 202, 1825 (2005). doi:10.1002/pssa.200520053.
11. D.J. Cohen, K.C. Ruthe, and S.A. Barnett, *J. Appl. Phys.* 96, 459 (2004). doi:10.1063/1.1760239.
12. T. Maemoto, N. Ichiba, S. Sasa, and M. Inoue, *Thin Solid Films* 486, 174 (2005). doi:10.1016/j.tsf.2004.10.057.
13. Dhananjay and S.B. Krupanidhi, *Appl. Phys. Lett.* 89, 082905 (2006). doi:10.1063/1.2266891.
14. D. Zhao, Y. Liu, D. Shen, Y. Lu, J. Zhang, and X. Fan, *J. Cryst. Growth* 234, 427 (2002). doi:10.1016/S0022-0248(01)01698-0.
15. C.S. Suchand Sandeep, R. Philip, R. Satheeshkumar, and V. Kumar, *Appl. Phys. Lett.* 89, 063102 (2006). doi:10.1063/1.2335375.
16. B.J. Norris, J. Anderson, J.F. Wager, and D.A. Keszler, *J. Phys. D: Appl. Phys.* 36, L105 (2003). doi:10.1088/0022-3727/36/20/L02.
17. H.C. Cheng, C.F. Chen, and C.Y. Tsay, *Appl. Phys. Lett.* 90, 012113 (2007). doi:10.1063/1.2404590.
18. J.H. Lee, P. Lin, C.C. Lee, J.C. Ho, and Y.W. Wang, *Jpn. J. Appl. Phys.* 44, 4784 (2005). doi:10.1143/JJAP.44.4784.
19. Y.J. Chang, D.H. Lee, G.S. Herman, and C.H. Chang, *Electrochem. Solid-State Lett.* 10, H135 (2007). doi:10.1149/1.2666588.
20. B.D. Cullity and S.R. Stock, *Elements of X-ray Diffraction* (New Jersey: Prentice-Hall, Inc., 2001), p. 388.
21. A. Ohtomo, M. Kawasaki, T. Koida, K. Masubuchi, H. Koinuma, Y. Sakurai, Y. Yoshida, T. Yasuda, and Y. Segawa, *Appl. Phys. Lett.* 72, 2466 (1998). doi:10.1063/1.121384.
22. G.W. Scherer, *J. Sol–Gel Sci. Tech.* 8, 353 (1997).
23. K.H. Kim, K.C. Park, and D.Y. Ma, *J. Appl. Phys.* 81, 7764 (1997). doi:10.1063/1.365556.
24. R.D. Tarey and T.A. Raju, *Thin Solid Films* 128, 181 (1985). doi:10.1016/0040-6090(85)90070-7.
25. S.T. Tan, B.J. Chen, X.W. Sun, W.J. Fan, H.S. Kwok, X.H. Zhang, and S.J. Chua, *J. Appl. Phys.* 98, 013505 (2005). doi:10.1063/1.1940137.
26. R.L. Hoffman, B.J. Norris, and J.F. Wager, *Appl. Phys. Lett.* 82, 733 (2003). doi:10.1063/1.1542677.
27. Dhananjay and S.B. Krupanidhi, *J. Appl. Phys.* 101, 123717 (2007). doi:10.1063/1.2748863.
28. H. Yabuta, M. Sano, K. Abe, T. Aiba, K. Nomura, T. Kamiya, and H. Hosono, *Appl. Phys. Lett.* 89, 112123 (2006). doi:10.1063/1.2353811.
29. J. Jo, O. Seo, H. Choi, and B. Lee, *Appl. Phys. Express* 1, 041202 (2008). doi:10.1143/APEX.1.041202.
30. J. Sun, D.A. Mourey, D.L. Zhao, and T.N. Jackson, *J. Electron. Mater.* 37, 755 (2008). doi:10.1007/s11664-007-0362-7.
31. T. Tsukada, *TFT/LCD: Liquid-Crystal Displays Addressed by Thin-Film Transistors* (Tokyo: Gordon and Breach Publishers, 1996), p. 59.